Particulate Infiltration into a Simulated Space Telescope

31 December 2008

De-Ling Liu and Kenneth T. Luey
Space Materials Laboratory
Physical Sciences Laboratories

Prepared for:

Space and Missile Systems Center
Air Force Space Command
483 N. Aviation Blvd.
El Segundo, CA 90245-2808

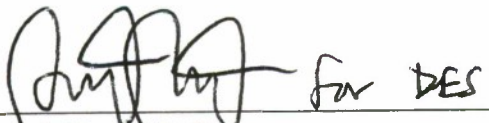Authorized by: Engineering and Technology Group

20090911249

AEROSPACE
Assuring Space Mission Success

Col. David E. Swanson
SMC/EA

REPORT DOCUMENTATION PAGE

Form Approved
OMB No. 0704-0188

1. REPORT DATE *(DD-MM-YYYY)*	2. REPORT TYPE	3. DATES COVERED *(From - To)*
31-12-2008		

4. TITLE AND SUBTITLE	5a. CONTRACT NUMBER
	FA8802-09-C-0001
Particulate Infiltration into a Simulated Space Telescope	5b. GRANT NUMBER
	5c. PROGRAM ELEMENT NUMBER

6. AUTHOR(S)	5d. PROJECT NUMBER
De-Ling Liu and Kenneth T. Luey	5e. TASK NUMBER
	5f. WORK UNIT NUMBER

7. PERFORMING ORGANIZATION NAME(S) AND ADDRESS(ES)	8. PERFORMING ORGANIZATION REPORT NUMBER
The Aerospace Corporation Physical Sciences Laboratories El Segundo, CA 90245-4691	TR-2009(8550)-3

9. SPONSORING / MONITORING AGENCY NAME(S) AND ADDRESS(ES)	10. SPONSOR/MONITOR'S ACRONYM(S)
Space and Missile Systems Center Air Force Space Command	SMC
483 N. Aviation Blvd. El Segundo, CA 90245	11. SPONSOR/MONITOR'S REPORT NUMBER(S)

12. DISTRIBUTION/AVAILABILITY STATEMENT

Approved for public release; distribution unlimited.

13. SUPPLEMENTARY NOTES

14. ABSTRACT

To understand the dynamics of airborne particulate intrusion into a space telescope, a mechanistic model based on mass balance was developed to predict the extent to which ambient particles penetrate through vent holes and enter the interiors after the purge is off. This work describes the mathematical modeling analysis, supplementing with results from laboratory measurements using a cylindrical chamber as a simulated space telescope. It was found that the characteristic time for airborne particles to reach a saturation level, after the purge is off, can be characterized by the air-exchange rate and particle deposition rate inside the confined space volume. The air-exchange rate, measured using a tracer gas technique, is associated with the natural convection and air flow turbulence intensity adjacent to the chamber. During the purge outage, the steady-state airborne particle concentration inside the space telescope is governed by the ambient particle concentration, air-exchange rate, and particle deposition rate.

15. SUBJECT TERMS

Particulate infiltration, Intrusion, Purge outage

16. SECURITY CLASSIFICATION OF:			17. LIMITATION OF ABSTRACT	18. NUMBER OF PAGES	19a. NAME OF RESPONSIBLE PERSON
					De-Ling Liu
a. REPORT	b. ABSTRACT	c. THIS PAGE		19	19b. TELEPHONE NUMBER *(include area code)*
UNCLASSIFIED	UNCLASSIFIED	UNCLASSIFIED			(310)336-0062

Standard Form 298 (Rev. 8-98)
Prescribed by ANSI Std. 239.18

Acknowledgments

Contents

Figures

Tables

1. Introduction

Purging is a common scheme to protect sensitive surfaces of payloads and spacecraft during testing, integration, and launch vehicle encapsulation. It provides particle-free gas (typically nitrogen) into the enclosed volume, preventing particle fallout onto contamination-sensitive surfaces by establishing a positive pressure. However, the purge is often turned off, either by processing plan or by inadvertent action. In the aerospace contamination control community, correlations developed by Buch and Barsh,[1] and Hamberg[2] are used to perform payload purge outage analysis in order to establish appropriate purge outage requirements. In reality, the transport of particles can be predicted by parameters that characterize air-exchange rate and particle deposition rate inside the space system volumes. In this report, a physical model is presented to provide the dynamic picture of particle intrusion into an enclosed space volume once the purge is turned off. Data of laboratory measurements from a simulated space telescope were obtained to validate our modeling predictions.

2. Method

2.1   Modeling Development

Assume an enclosed volume, such as a space telescope (ST), is purged to positive pressure by a gaseous nitrogen (GN_2) flow. When the purge is on, the airborne particulate level inside the enclosure is usually very low. When the purge is turned off, the ambient airborne particles are transported into the enclosure owing to random thermal motions of air molecules as well as natural convection in the presence of a temperature gradient. Particles infiltrate through the designed vent holes as well as unintentional leakage paths. Inside the enclosure, the airborne particle concentration change as a function of time can be represented by the following equation:

$$\frac{dC_{in}}{dt} = p\lambda C_{out} - (\lambda + k)C_{in},$$ (1)

where C_{in} and C_{out} are the airborne particle number concentration inside and outside the control volume (CV; mass/cm^3 or #/cm^3), respectively, p is the particle penetration factor (dimensionless) through the leaks of CV, λ and k are the air-exchange rate (Volume Air Changes per Hour, ACH, h^{-1}) and particle deposition rate (h^{-1}) onto interior surfaces of the CV, respectively. The schematic representation of the mathematical model is illustrated in Figure 1. A detailed configuration of the payload is not required for the current modeling analysis; here, a cylindrically shaped enclosure is used to represent a space telescope.

Equation (1) is the mass balance equation, which simply states that the rate of airborne particle concentration change inside the CV is governed by a *source* term, $p\lambda C_{out}$, and a *sink* term, $(\lambda + k)C_{in}$. In the schematic shown in Figure 1, the *source* term is the infiltration of particles from the exterior ambient environment into the CV by making perhaps one or more right-angle turns into the CV at an air-exchange rate of λ. The *sink* term refers to the processes in which airborne particles inside CV, C_{in},
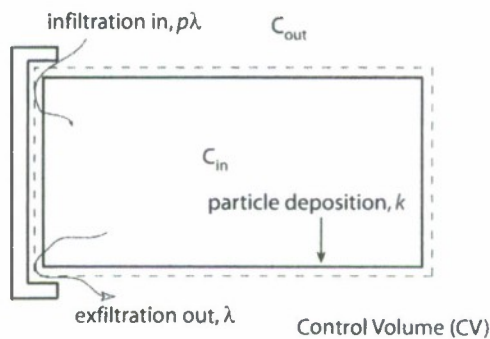

Figure 1.   Schematic representation of the air exchange (infiltration and exfiltration), as well as particle deposition loss components in the mechanistic model.

are removed by means of exfiltration, λC_{in}, and deposition loss, kC_{in}. Exfiltration is the particle removal mechanism in which airborne particles are swept out of the CV by air exchange, and deposition loss is the mechanism in which airborne particles deposit onto interior surfaces of CV by gravity, diffusion, and perhaps other particle deposition mechanisms. Exfiltration and deposition loss, which are two independent processes, occur at the same time. In addition, both mechanisms are well approximated as a first-order process, thus λ and k are linearly proportional to C_{in}.[3]

We will use the following several paragraphs to elaborate the important parameters involved.

2.1.1 Particle Deposition Rate, k

Note that particle size plays a major role in every aspect of aerosol behavior, such as the rate of deposition onto surfaces. Therefore, it is necessary in Eq. (1) to take particle size into account. This was treated by segregating particles into various size bins. Lai[4] compiled a review of particle deposition rate k as a function of particle size under various settings, including the ratio of surface area to volume and airflow turbulence intensity. The distinct feature of particle deposition behaviors is that particles of 0.1–2 μm in aerodynamic diameters have the lowest deposition rates in comparison to particles smaller and larger than this size range. This means that particles of 0.1–2 μm tend to linger in air and remain airborne longer than particles < 0.1 μm and > 2 μm. Particles smaller than 0.1 μm are more readily removed by Brownian and turbulent diffusion, and particles larger than 2 μm are more effectively removed by gravitational settling.

2.1.2 Air-Exchange Rate, λ

Air displacement out of the control volume, exfiltration, plays a role in removing particles, and this removal process is characterized by air-exchange rate. Air-exchange rates can be calculated as the ratio of air flowrate into (or out) of the space versus the enclosure volume under isothermal conditions in which the air volume does not expand or contract. When the CV geometry is not well defined and/or the air flowrate is hard to measure, the air-exchange rate can be determined using tracer gas techniques.[5] In this manner, the air-exchange rate arises as an aggregate term to characterize the overall rate of air replenishment through all leaks and openings on the envelope of a control volume; therefore, detailed information on the geometry of the leakage paths is not required. Air-exchange rate usually can be used to evaluate the effectiveness of airborne contaminant removal by means of the ventilation process. Particle removal by air exchange occurs at a rate independent of particle size.

2.1.3 Penetration Factor, p

The penetration factor, p, is the fraction of particles that is transported by the infiltrating air and remains airborne as air enters the control volume. The value of p may vary depending on the residence time within the leakage path, which is governed by leak dimensions and pressure differential across the openings. As expected, p is a function of particle size, and its values can be calculated for well-defined, simplified leakage geometries.[6] For complicated leakage geometries, the value of p can only be determined by experiments. For particles with aerodynamic diameter smaller than 10 μm, particle penetration is expected to be complete (i.e., p = 1) when the air velocity within the leaks is low.[7,8] When the leakage height is less than 1 mm, particles larger than 10 μm are more likely to set-

4

tle onto the surfaces by gravity along the leakage path ($p < 1$). Thus, particle penetration is considered complete unless the control volume is made extremely air-tight (e.g., leak path height < 1 mm).

2.1.4   Solution to the Mass Balance Equation

Assuming C_{out}, λ, and k are constant over time, and the initial aerosol concentration inside the control volume is zero (i.e., $C_{in} = 0$ at time zero), the time-dependent particle concentration inside the control volume, $C_{in(t)}$, can be expressed as the analytical solution to Eq. (1):

$$C_{in}(t) = \frac{p\lambda}{\lambda + k} C_{out} \left[1 - \exp\left(-(\lambda + k)t \right) \right] \tag{2}$$

Under the circumstances in which C_{out}, λ, and k vary with time, a numerical multi-step approach for the transient mass-balance analysis can be performed to solve $C_{in(t)}$. Here, such complexities are omitted in order to focus on the physical implications of the particle transport processes. The interpretation of Eq. (2) will be elaborated in the Results section along with experimental data.

In summary, a mechanistic view of airborne particle transport into space system volumes through infiltration and their fate—deposition loss onto surfaces and exfiltration with outgoing air—can be represented by a material balance equation. From the perspective of contamination control, particle deposition onto surfaces is the undesirable outcome and should be minimized as much as possible. Based on the understanding of the particle transport processes as well as the nature of air infiltration into space system volumes, a mathematical model can be applied to seek the important parameters that affect the extent of particle intrusion and their fallout.

2.2   Experimental Validation

2.2.1   Experimental Apparatus

A simulated space telescope (SST) was designed and constructed using an acrylic cylindrical tube and materials. The schematic is illustrated in Figure 2. The front cover (to the left) is designed such that a
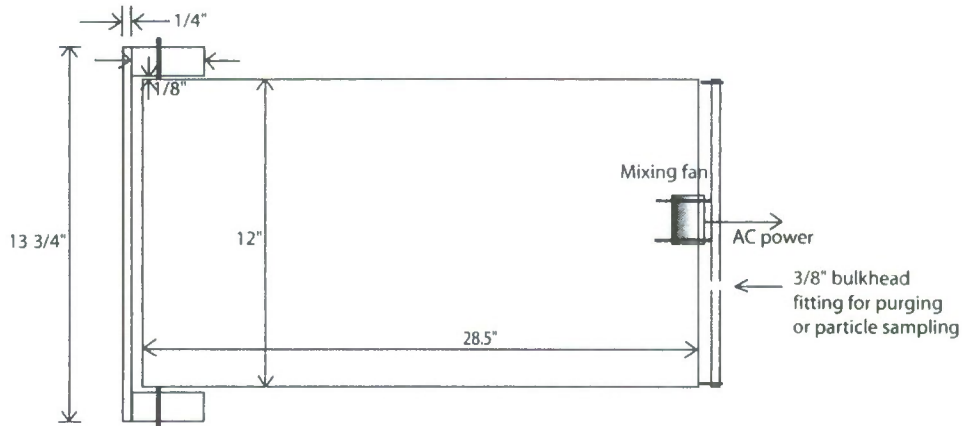

Figure 2.   Side view of the simulated space telescope (SST) apparatus schematic.

maximum leakage clearance of 1/8 in. ("most open") can be achieved yet complete closure can also be achieved by pushing the cover all the way to the end ("most closed"). A fan was installed inside the SST to promote air mixing to meet the need of experiments when necessary.

2.2.2   Air-Exchange Rate Measurements

The rate of air displacement within the SST can be characterized in terms of air-exchange rate. A tracer gas technique was employed to determine the air-exchange rate. The concept of a tracer gas technique is to generate a uniform concentration throughout the enclosure by a brief pulse addition of tracer gas into the enclosure. Once the tracer gas source has exhausted, the concentration is diluted over time owing to the replenishment of air from the exterior ambient environment that contains no tracer gas. The rate of tracer gas concentration change can be described by

$$\frac{dC}{dt} = -\lambda \, C \, , \tag{3}$$

where C is the tracer gas concentration, and λ is the air-exchange rate. After rearrangement, Eq. (3) becomes

$$\ln C_{(t)} - \ln C_{(0)} = -\lambda t, \tag{4}$$

where $C_{(0)}$ and $C_{(t)}$ are the tracer gas concentration inside SST at time 0 and t, respectively. When the air is well-mixed, plotting lnC as a function of time gives rise to a linear plot with the slope yielding the air-exchange rate λ.

With respect to the selection of a tracer gas, SF_6 is an ideal candidate due to its extremely rare presence in the atmosphere, but its detection requires GC/ECD (gas chromatography equipped with electron capture detector, down to ppt level), or nondispersive IR absorption (at ppm level). Neither was available during the time frame of our experiments. Instead, CO_2 was used as the alternative because of its approximately constant concentration in the ambient environment. Furthermore, CO_2 monitors are economical and readily available.

A CO_2 monitor (Telaire 7001, Engelhard) was placed inside the SST to measure CO_2 concentrations with time. A pulse of CO_2 was generated from a CO_2 gas cylinder (Scott Specialty Gases) connected to the SST with a tubing. In the case when particle measurements were not involved, the fan inside the SST was turned on briefly for 5–10 s to mix the air and CO_2, and turned off immediately. It is found that the use of mechanical mixing, even turning on a fan briefly, can artificially enhance particulate infiltration owing to the increased level of convection. In the experiments, two options of front-cover layout were selected: 1/8 in. clearance around the SST opening (most open), and complete closure (most closed). These two configurations were chosen to evaluate the upper and lower bounds of air-exchange rates associated with the SST configuration.

6

2.2.3 Particle Measurements

As mentioned earlier, purging is a common scheme to protect sensitive surfaces from contamination inside space system volumes. Therefore, it is important to predict how long it takes for ambient particulates to infiltrate into a space system volume when the purge is taken away either by design or unintentionally.

Figure 3 shows the schematic for measuring airborne particle concentrations with respect to the experimental setup. The SST is purged with filtered, particle-free air (HEPA capsule, Pall Life Sciences) until the measured particle concentrations inside the SST were reduced to a negligible level. With the front cover oriented in the designated fashion ("most open" or "most closed"), the purged air was stopped, and the ambient air was allowed to bring in the particles from outside the SST via natural convection. The particle concentrations inside and surrounding the SST were determined using a laser optical particle counter (Aerodynamic Particle Spectrometer, APS, Model 3321, TSI, Inc.). In addition to measuring light scattering intensities, the APS sizes particles using a time-of-the-flight technique that determines aerodynamic diameters in real time. Equipped with highly resolved particle sizing capabilities, APS reports particle concentrations in 52 channels from 0.5 to 20 μm.

In the infiltration experiments, no airborne particles were generated artificially for providing particles; instead, the ambient airborne particles were used as the particle source.

During the course of particle infiltration experiments, it is desirable to withdraw aerosol samples from the SST with a low air flowrate to minimize perturbations of the system, where natural convection is the mechanism for particle intrusion. To do so, particle-free makeup air at a fixed flowrate (0.9 lpm), regulated by a mass flow controller (MKS Instruments, Inc.), is supplied together with air samples (0.1 lpm) from the SST to APS (1.0 lpm total for aerosol flow). Therefore, only ~0.4% of SST air volume was withdrawn over the two 1-min aerosol sampling periods. In addition, a 3-way valve was in place, as illustrated in Figure 3, so that the aerosol concentrations adjacent to the SST, C_{out}, and that inside the SST, C_{in}, can be measured sequentially. The tubing diameters and lengths for sampling C_{in} and C_{out} were made identical so that the corresponding aerosol loss in the sampling lines was the same.
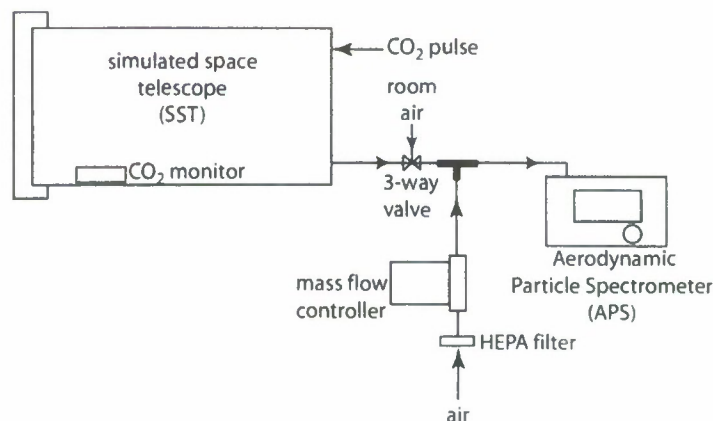
Figure 3. Experimental schematic for measuring particle infiltration into a simulated space telescope (SST).

The sequence of experimental runs involved the following steps: (1) purge the SST with HEPA-filtered air; (2) inject CO_2 after the airborne particles inside the SST has reached a negligible level; (3) stop purge and let CO_2 mix homogeneously by the remaining purge air momentum and natural convection; (4) take 1-min aerosol samples and the duplicates periodically from the SST (C_{in}) and the adjacent environment (C_{out}), respectively.

3. Results and Discussion

3.1   Measurements of Air-exchange Rate

Air-exchange rates of the SST were evaluated under two different locations: an unoccupied office and a clean room. They were used to represent different air turbulence intensities in the surrounding environments. The front cover was set at two closure conditions: "most closed" when the cover touches the STT, and "most open" when the minimum opening is at ~ 1/8 in. clearance.

Figure 4 shows a typical CO_2 concentration decay as a function of time, and a linear regression was performed to calculate the slope, which yielded the air-exchange rate. Note that when CO_2 is used as a tracer gas for air-exchange rate calculations, the background ambient CO_2 concentration was sub-tracted from the measured values prior to evaluating the decay rate. Good air mixing inside the SST was indicated by the linear relationship of the logarithmic values of CO_2 concentration versus time.

The measured air-exchange rates are summarized in Table 1. Experiments O-1 to O-4 and C-1 to C-3 were performed in an unoccupied office and a clean room, respectively. Two CO_2 monitors were placed inside the SST, one at the left end and the other at the right end, to evaluate whether the air-exchange rates are different locally in the absence of mechanical mixing.
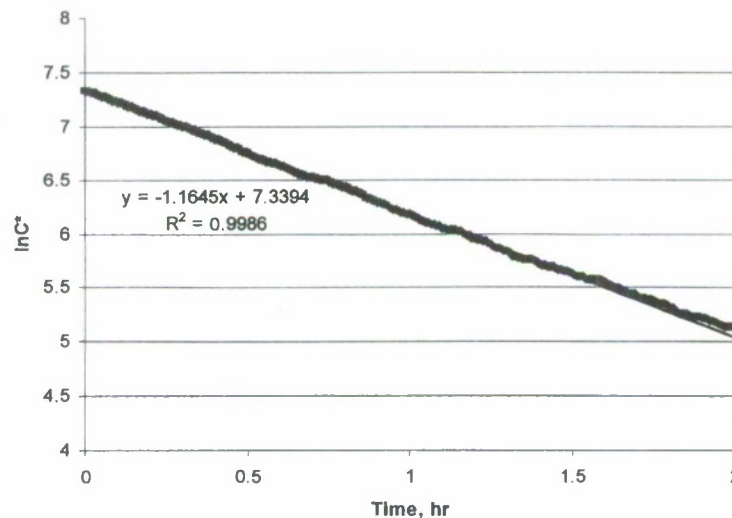

Figure 4.   Air-exchange rate measured by concentration decay of CO_2 in an unoccu-
pied office with the door closed (experiment O-3 in Table 1). The con-
centration C^* is background corrected as $C^* = [CO_{2(t)} - CO_{2,b}]$.

The following conclusions are drawn from the ACH measurements:

1. The differences of ACH measured at two different locations within the SST were insignificant, which means that the two sampling locations were subject to nearly identical air-exchange rate. Therefore, only one monitor was used in the final two tests (O-4 and C-3) and the subsequent particle infiltration experiments.

2. In the unoccupied office setting, the air was usually calm and not drafty. On the other hand, the airflow in the clean room was evidently more turbulent. When the opening leakage area was left the same, the measured ACH in the clean room was roughly two times higher than that in the unoccupied office, as shown in the paired experiments O-3 vs. C-1 and O-4 vs. C-3. In other words, air flow turbulence intensity adjacent to the SST plays a role in determining how fast the ambient air infiltrates into the SST.

3. Under the same settings (either unoccupied office or clean room), it is clearly seen that the measured upper bound ACHs ("most open") was one order of magnitude greater than the lower bound counterparts ("most closed"), as indicated in the paired experiments O-3 vs. O-4 and C-1 vs. C-3. This difference in ACHs was attributed to the available leakage area allowed for air infiltration. Therefore, air exchange between the enclosure and the surroundings can be minimized by making leakage areas as small as possible.

Table 1. Summary of Air-Exchange Rates (ACH) Inside the SST Measured by the CO_2 Tracer Gas Technique Under Various Settings. The front cover was usually left at "most open" configuration (~1/8 in. clearance) unless specified by [v].

ACH, h^{-1}	O-1	O-2	O-3	O-4[v]	C-1	C-2	C-3[v]
#1	1.9	1.3	1.2	0.1	2.7	2.8	0.2
#2	2	1.6	1.2		2.7		

#1, #2: two CO_2 monitors placed at two different locations (left and right) inside the SST
O-1: with office door open and occasional people's movement
O-2: with office door closed (most of the time; somebody came in and stayed for 40 min, but it did not seem to influence the result)
O-3: with office door closed and run overnight
O-4: with office door closed and front cover most closed
C-1: in clean room
C-2: in clean room and use one monitor only
C-3: in clean room, using one monitor and with front cover most closed
[v] "most closed" configurations
[.] #2 data logger not activated

3.2   Modeling Analysis on Particle Infiltration

As mentioned in Subsection 2.1, the dynamics of particle transport from the ambient environment into the control volume can be analyzed using a mechanistic model, as demonstrated by Eq. (1). The key parameters are air-exchange rate (ACH), λ, and particle deposition coefficient, k, where k is a function of particle size. Thus, one should expect that the extent of particle concentration rise due to infiltration would vary according to particle sizes.

According to the mathematical expression of Eq. (2), Figure 5 illustrates the predicted particle concentration growth with time under several different postulated scenarios in which ACH, λ, and various particle deposition rates, k, were assumed. After rearrangement and assuming p = 1, Eq. (2) becomes
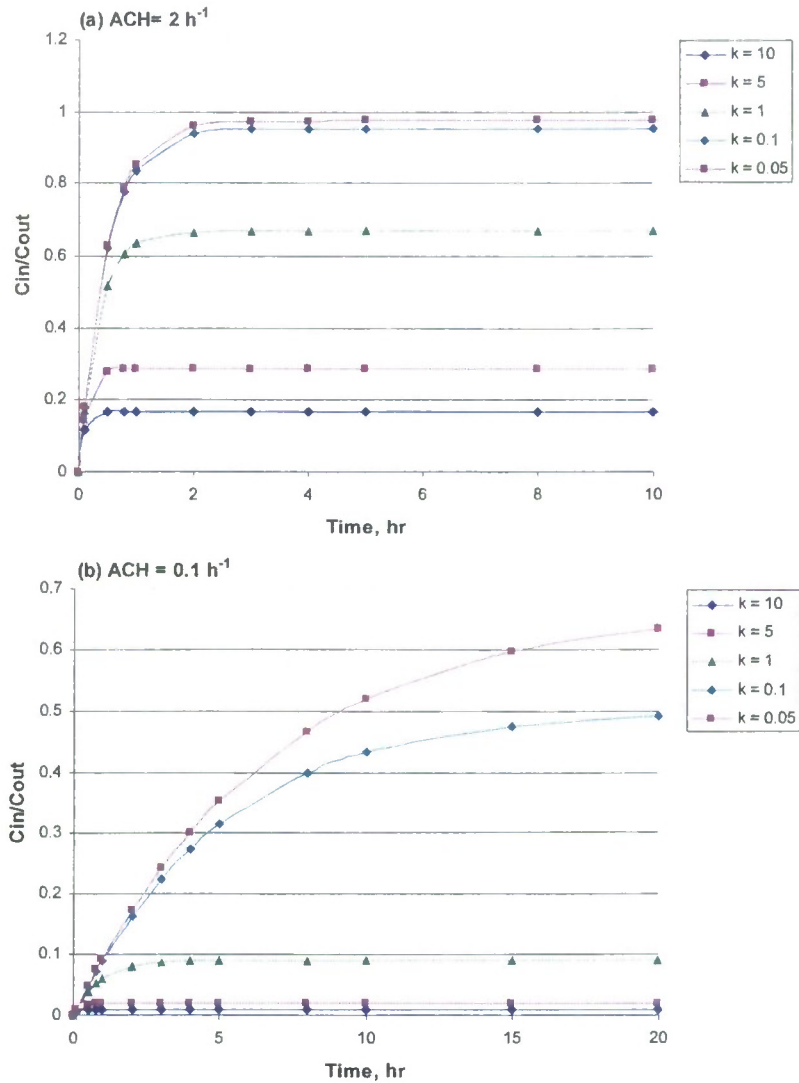
Figure 5. The growth of particle concentrations inside the SST as a function of time predicted by Eq. (7), which is the analytical solution of the governing equation describing particle infiltration into the SST. Five different particle deposition rates k from 0.05 to 10 h⁻¹ under ACH of 2 and 0.1 h⁻¹ were considered in this modeling analysis.

$$\frac{C_{in}(t)}{C_{out}} = \frac{\lambda}{\lambda + k}\left[1 - \exp(-(\lambda + k)t)\right] \qquad (5)$$

Five particle deposition rates ranging from 0.05 to 10 h⁻¹ were used under ACHs of 0.1 and 2 h⁻¹, which, in terms of order of magnitude, represent the air exchange obtained from the prior tracer gas experiments when the cover was at "most closed" and "most open" configurations. Depending on the surface area-to-volume ratio (S/V),[1] 0.2–1 h⁻¹ is the range of particle deposition rate for 0.3-μm parti-

_____

[1] S/V is used as a normalized indicator of available surfaces for particle deposition.

11

cles, and 10 h^{-1} or higher is a reasonable approximation for 5-μm particles inside an enclosure such as SST.[4] This mathematical analysis is helpful to gain insights into the relative importance of air exchange and particle deposition to the overall concentration-time profile since they are the two competing mechanisms responsible for airborne particle loss in the SST.

From Figure 5(a), it is evident that after a certain time frame, particle concentrations grow from zero to a fixed level—a *steady-state* concentration. By definition, the steady-state concentration does not change with time, and the value can be estimated as

$$C_{in} = \frac{\lambda}{\lambda + k} C_{out} \tag{6}$$

or

$$\frac{C_{in}}{C_{out}} = \frac{\lambda}{\lambda + k} \tag{7}$$

when t in Eq. (5) goes to infinity. At steady state, the particles brought into the SST from exterior ambient air (λC_{out}, the source term) is balanced by airborne particle loss inside the SST due to deposition onto the surfaces and air exchange that sweeps particles out (kC_{in} and λC_{in}, the sink terms).

Another distinct feature from the mathematical analysis as shown in Figure 5 is the curvature for the concentration rise, which can be captured by the parameter of *characteristic time* τ, given by

$$\tau \sim \frac{1}{\lambda + k}, \tag{8}$$

where τ is the time, in hours, required for the system to relax from its initial condition to the steady state.

Table 2. Characteristic Times and Steady-State C_{in}/C_{out} Calculated in the Postulated Particle Infiltration Scenarios Based on the Mathematical Model Analysis

Particle Deposition Rate k, h^{-1}	Air-exchange Rate λ, h^{-1}			
	0.1		2	
	τ, hr	C_{in}/C_{out}	τ, hr	C_{in}/C_{out}
0.05	6.7	0.67	0.49	0.98
0.1	5.0	0.5	0.48	0.95
1	0.9	0.09	0.33	0.67
5	0.2	0.02	0.14	0.29
10	0.1	0.01	0.08	0.17

Table 2 gives a summary of τ values as well as the steady-state C_{in}/C_{out} ratio associated with the above hypothetical scenarios. It can be seen that given the same k, it is predicted to take less time for the system with higher ACH to reach the steady state. For instance, assuming $k = 1\ h^{-1}$, the characteristic times estimated to establish steady state are 0.9 h for ACH = 0.1 h^{-1}, and ~0.3 h for ACH = 2 h^{-1} system, respectively. However, this discrepancy in characteristic time is not as pronounced when k becomes dominant; i.e., particle deposition becomes the important mechanism to control how fast particles are removed from the system. Furthermore, one can also see that greater values of k, as would be the case for larger particles, also lead to more particle fallout, as a result, lowering the steady-state C_{in}/C_{out} ratios.

Particle deposition rate, k, is governed by particle size as well as the degree of airflow turbulence *inside* the control volume; higher turbulence intensity results in greater particle deposition rate owing to stronger near-surface air flow conditions.[3,9] Therefore, a quiescent air flow condition is expected to result in a smaller k, which is advantageous when minimized particle fallout is the goal. In addition, reducing air exchange between the control volume and the ambient environment would be a favorable approach (assuming the CV itself is clean, free of particles, and the exterior ambient environment contains particles). Lower air exchange can delay the progress for airborne particles to infiltrate into the system.

3.3   Model Validations

Particle infiltration experiments were conducted in the laboratory to compare with the modeling predictions. Throughout the infiltration experiments, the SST was located in a small, unoccupied laboratory space where the ventilation was centrally controlled by the building. The air-exchange rates were measured simultaneously during the early particle infiltration progress, with the details of experimental setup and procedures described in Subsection 2.2.3. With a CO_2 pulse injected as the tracer gas, the ACHs under the unoccupied laboratory setting were determined to be approximately 0.1 and 1 h^{-1} when the SST were in the configurations of "most closed" and "most open," respectively. After the SST purge was off, the ratios of C_{in}/C_{out} as a function of particle size were determined from C_{in} and C_{out} measurements by APS. The power along with the air pumping action of APS were turned off when not measuring C_{in} or C_{out} in order to minimize its air convection interference on the air exchange of SST.

Figure 6 illustrates the comparison of modeling calculations and the laboratory results from the particle infiltration experiments. In the figures, the symbols of different shapes indicate the measured C_{in}/C_{out} ratios of different particle size range under the indicated ACH settings, and the lines were obtained from the model calculations based on three sets of particle deposition rates ($k = 0.4, 0.8$, and 1.5 h^{-1}), which were used to represent the plausible particle deposition rate of 0.5–2 μm particles under the quiescent airflow characteristics inside the SST (estimated from complied data in referece [4]). In the air-tight "most closed" setting where the ACH was measured at ~0.1 h^{-1}, the experimental data agreed well with the model predictions, as shown in Figure 6(a). In the less air-tight "most open" setting, the data followed the model predictions fairly well, although few exceptions existed, as seen in Figure 6(b).

In modeling calculations, the C_{in}/C_{out} ratios were evaluated from particle deposition rates of 0.4, 0.8, and 1.5 h^{-1} in combination of ACHs of 0.1 and 1 h^{-1}, as suggested in Eq. (7). Therefore, both the
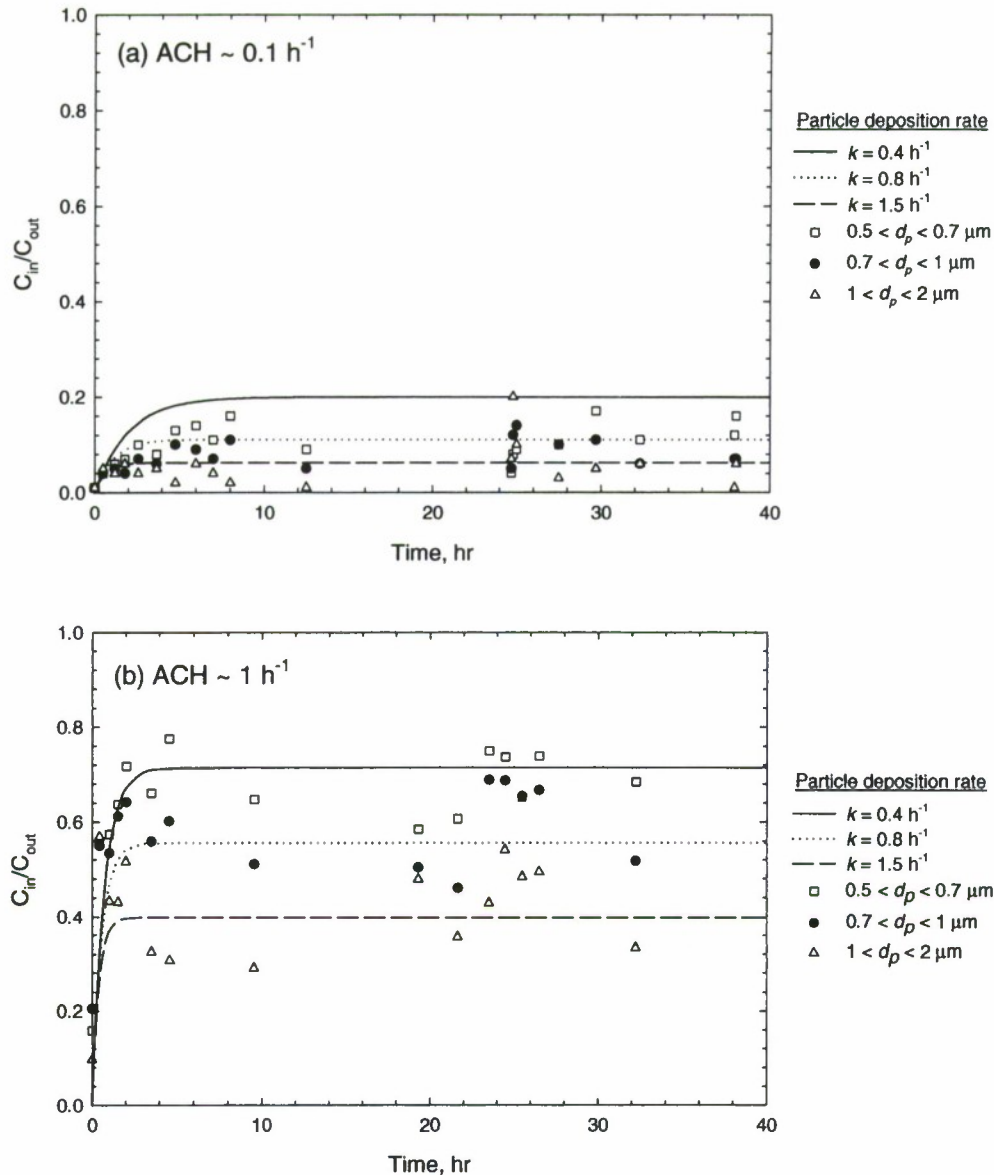
Figure 6. Comparison of modeling calculations with laboratory data in the SST particle infiltration experiments under (a) ACH ~0.1 h^{-1}, and (b) ACH ~1 h^{-1}. The values of ACH were obtained using CO_2 tracer gas decay method. Three sets of k, 0.4, 0.8, and 1.5 h^{-1}, were used in the model calculation to bound the likely range the airborne particle loss rate due to deposition.

values of ACH and particle deposition rate play a role in determining C_{in}/C_{out}. In Figure 6(b), the data beyond the range predicted by the model ($0.4 \leq C_{in}/C_{out} \leq 0.7$) may be attributed in part by the fact that the actual ACH fluctuated throughout the course of infiltration experiments owing to air-conditioning changes in the building. In the less air-tight "most open" configuration, the correlation between SST ACHs and building ventilation conditions was observed. For example, ACHs of ~2 and ~3 h^{-1} were measured when the building ventilation system was set in higher output of airflow into the laboratories in response to outdoor weather change (particle infiltration experiments were not per-

14

formed during this time). On the other hand, such correlations were not as pronounced when the STT was in the air-tight "most closed" configuration. This is because the air exchange is strongly influenced by the extent of surrounding air that comes in and replenishes the old air inside the SST. Therefore, the more air leakage area available on the SST as in the case of "most open" scenario, the more likely the air exchange would be more significantly affected by the surrounding air flow characteristics (e.g., ventilation settings). All of these are consistent with the experimental observations described in Subsection 3.1.

In addition to the ACH values, the particle deposition rate, k, used in the model will also alter C_{in}/C_{out} ratios predicted in the model. To arrive at the some of the measured C_{in}/C_{out} values under the "most open" scenario, it is likely that the actual k values were slightly less than 0.4 h^{-1} for 0.5–0.7 μm particles, and slightly greater than 1.5 h^{-1} for 1–2 μm particles. In fact, particle deposition is a complicated transport process; thus, the magnitude of deposition rates depends on factors that govern particle transport, such as particle size, the near-surface air turbulence, surface characteristics including orientation and texture (smooth vs. rough), air-surface temperature difference, and the presence of electrical field on the surface.[4,10] In other words, there is no single universal particle deposition rate applicable to all settings. Nevertheless, a reasonable range of deposition rates can be applied in modeling analyses to gain insights into the plausible particulate infiltration scenarios as well as particulate surface accumulation over time.

4. Conclusions

A modeling analysis and experimental work were conducted to provide physical insights into the dynamics of airborne particle transport into a generic confined space system volume. A mechanistic model based on material balance was employed to account for the particle transport processes by means of air exchange and particle deposition onto interior surfaces. The analytical results show that the airborne particle concentration change inside the control volume is governed by two parameters: *air-exchange rate* (ACH) λ, and *particle deposition rate k*. The air-exchange rate can be measured using a tracer gas technique as demonstrated in this report, and the size-specific particle deposition rates can be determined experimentally, or approximated from the existing literature.

The experiments for model validations were performed in two ACH settings: 0.1 and 1 h^{-1}. From the data it can be seen that after the purge is off, the particle concentration increases with time until it reaches a steady state, which stays at a constant level relative to the ambient particle concentration and does not change with time. The pace of particle concentration increase can be approximated by the parameter of *characteristic time*, τ, which is associated with λ and k, as indicated in Eq. (8). The steady-state particle concentration is governed by λ and k, as well as the ambient concentration C_{out}, as shown in Eq. (6). The experimental data agree relatively well with the modeling predictions.

This simple mathematical model is applicable not only in scenarios such as particulate intrusion into a space telescope during purge outage, but also in cases where particle infiltration into payload fairing when environmental control system (ECS) air interruption occurs. More effort will be needed to characterize size-specific particle deposition rate under the air flow conditions representing the actual degree of turbulence inside space system volumes while air-exchange rates are measured simultaneously. Particle fallout rates yielded from such deposition experiments are expected to help elucidate the time-dependent correlation between air cleanliness class and surface particle cleanliness level, and to further establish physical-based purge outage requirements.

5. References

1. Buch, J. D. and Barsh, M. K., "Analysis of particulate contamination buildup on surfaces," *SPIE proceedings: optical system contamination: effect, measurement, control*, 1987, 777: 43–54.

2. Hamberg, O., "Particle fallout predictions for clean rooms," *Journal of Environmental Science*, 1982, 25:15.

3. Nazaroff, W. W. and Cass, G. R., "Mass-transport aspects of pollutant removal at indoor surfaces," *Environment International*, 1989, 15: 567–584.

4. Lai, A. C. K., "Particle deposition indoors: a review," *Indoor Air*, 2002, 12: 211–214.

5. "Standard test methods for determining air exchange in a single zone by means of a tracer gas dilution," American Society for Testing and Materials, ASTM E741-93, 1993, 625–640.

6. Liu, D.-L. and Nazaroff, W. W., "Modeling Pollutant Penetration Across Building Envelopes," *Atmospheric Environment*, 2001, 35, 4451–4462.

7. Liu, D.-L. and Nazaroff, W. W., "Particle Penetration through Building Cracks," *Aerosol Science and Technology*, 2003, 37, 565–573.

8. Liu, D.-L., "Air pollutant penetration through airflow leaks into buildings," Ph.D. dissertation, University of California at Berkeley, 2002.

9. Thatcher, T. L., Lai, A. C. K., Moreno-Jackson, R., Sextro, R. G., and Nazaroff, W. W., "Effects of room furnishings and air speed on particle deposition rates indoors," *Atmospheric Environment*, 2002, 36: 1811–1819.

10. Nazaroff, W. W., Gadgil, A. J., and Weschler, C. J., "Critique of the use of deposition velocity in modeling indoor air quality," *Modeling of Indoor Air Quality and Exposure*, ASTM STP 1205 (N. L. Nagda, ed.), American Society for Testing and Materials, Philadelphia, 1993, 81–104.

PHYSICAL SCIENCES LABORATORIES

The Aerospace Corporation functions as an "architect-engineer" for national security programs, specializing in advanced military space systems. The Corporation's Physical Sciences Laboratories support the effective and timely development and operation of national security systems through scientific research and the application of advanced technology. Vital to the success of the Corporation is the technical staff's wide-ranging expertise and its ability to stay abreast of new technological developments and program support issues associated with rapidly evolving space systems. Contributing capabilities are provided by these individual organizations:

Electronics and Photonics Laboratory: Microelectronics, VLSI reliability, failure analysis, solid-state device physics, compound semiconductors, radiation effects, infrared and CCD detector devices, data storage and display technologies; lasers and electro-optics, solid-state laser design, micro-optics, optical communications, and fiber-optic sensors; atomic frequency standards, applied laser spectroscopy, laser chemistry, atmospheric propagation and beam control, LIDAR/LADAR remote sensing; solar cell and array testing and evaluation, battery electrochemistry, battery testing and evaluation.

Space Materials Laboratory: Evaluation and characterizations of new materials and processing techniques: metals, alloys, ceramics, polymers, thin films, and composites; development of advanced deposition processes; nondestructive evaluation, component failure analysis and reliability; structural mechanics, fracture mechanics, and stress corrosion; analysis and evaluation of materials at cryogenic and elevated temperatures; launch vehicle fluid mechanics, heat transfer and flight dynamics; aerothermodynamics; chemical and electric propulsion; environmental chemistry; combustion processes; space environment effects on materials, hardening and vulnerability assessment; contamination, thermal and structural control; lubrication and surface phenomena. Microelectromechanical systems (MEMS) for space applications; laser micromachining; laser-surface physical and chemical interactions; micropropulsion; micro- and nanosatellite mission analysis; intelligent microinstruments for monitoring space and launch system environments.

Space Science Applications Laboratory: Magnetospheric, auroral and cosmic-ray physics, wave-particle interactions, magnetospheric plasma waves; atmospheric and ionospheric physics, density and composition of the upper atmosphere, remote sensing using atmospheric radiation; solar physics, infrared astronomy, infrared signature analysis; infrared surveillance, imaging and remote sensing; multispectral and hyperspectral sensor development; data analysis and algorithm development; applications of multispectral and hyperspectral imagery to defense, civil space, commercial, and environmental missions; effects of solar activity, magnetic storms and nuclear explosions on the Earth's atmosphere, ionosphere and magnetosphere; effects of electromagnetic and particulate radiations on space systems; space instrumentation, design, fabrication and test; environmental chemistry, trace detection; atmospheric chemical reactions, atmospheric optics, light scattering, state-specific chemical reactions, and radiative signatures of missile plumes.